Numerical Investigation Of Reinforcement Ratio Effects on the Flexural Performance of High-Calcium Fly Ash Geopolymer Concrete Beams

Muhammad Rifky Trisnawardhana [1], Bambang Piscesa[2], Indra Komara[3]
[1,2]Civil Engineering Department, Institut Teknologi Sepuluh Nopember (ITS) Surabaya, Surabaya
[3]Civil Engineering Department, Institut Teknologi Adhi Tama Surabaya (ITATS), Surabaya

Email: [1]rifkytrisna021@gmail.com, [2]piscesa@ce.its.ac.id, [3]indrakomara@itats.ac.id

Received: 2025-12-24 Received in revised from 2026-01-30 Accepted: 2026-03-11

Abstract

This study investigates the influence of the longitudinal reinforcement ratio on the flexural behavior of high-calcium fly ash geopolymer concrete (GPC) beams using three-dimensional nonlinear finite element analysis (3D NLFEA). Beams with identical geometry and shear reinforcement were modeled, with reinforcement ratios varied from under-reinforced to over-reinforced conditions. Material properties were based on validated experimental data. Results show that increasing reinforcement enhances flexural strength but significantly reduces ductility and energy absorption. Under-reinforced beams exhibited ductile, tension-controlled failure governed by steel yielding, while over-reinforced beams failed abruptly due to concrete crushing. The transition from ductile to brittle behavior occurs at significantly lower reinforcement ratios in GPC (around $\rho = 0.0157$) compared to ordinary Portland cement concrete. Based on ductility ratio, energy absorption, and toughness index i_{10}, a maximum reinforcement ratio of $\rho \leq 0.010$ is recommended for ductile design of high-calcium fly ash GPC beams.

Keywords: *Ductility; Finite element analysis; Flexural behavior; Geopolymer concrete; Reinforcement ratio*

1. Introduction

Concrete is the most widely used construction material globally. However, its heavy reliance on ordinary Portland cement (OPC) contributes significantly to global carbon emissions, with the cement industry alone responsible for nearly 8% of worldwide CO_2 emissions [1]. In response, researchers have explored more sustainable alternatives such as geopolymer concrete (GPC), which is developed through alkali activation of aluminosilicate-rich materials like fly ash or slag [2], [3].

High-calcium fly ash-based GPC offers advantages such as rapid strength gain and stable mechanical properties under ambient curing [4], [5]. Studies show that GPC possesses high compressive strength, low permeability, and excellent resistance to chemical attack [6]-[8]. However, its flexural behavior differs considerably from conventional OPC concrete, with lower tensile strain capacity and reduced post-cracking ductility [9], [10].

A critical knowledge gap exists regarding the quantitative influence of longitudinal reinforcement ratio on the flexural ductility and failure mode transition of high-calcium fly ash GPC beams. While extensive research has focused on mix design and compressive strength, studies examining reinforcement ratio effects remain limited. Research by Sarker [11] and Nath & Sarker [5] highlighted that conventional design provisions from codes such as SNI 2847:2019 [12] or ACI 318 [13] tend to overpredict ductility when applied directly to GPC. Numerical investigations by Wibowo & Piscesa [14] demonstrated that stress distribution and crack propagation in GPC beams deviate from OPC systems.

This study addresses that gap by investigating the flexural behavior of high-calcium fly ash geopolymer concrete beams with varying longitudinal reinforcement ratios using three-dimensional nonlinear finite element analysis (3DNLFEA). The results are compared with existing code limits to assess their applicability to geopolymer concrete and provide insight into developing more accurate, performance-based design criteria.

2. Method

The research methodology began with collecting reference data and material parameters from previous validated studies on reinforced geopolymer concrete beams [5], [11], [14]. Beam geometry, reinforcement details, and material properties were adapted to ensure accurate simulation of flexural performance under four-point bending.

2.1. Test Speciment And Material Data

All specimens were modeled as simply supported beams with a rectangular cross-section of 200 mm × 300 mm, spanning 2700 mm. The loading configuration simulated a four-point bending test to produce a constant-moment region in the middle third of the span. Longitudinal reinforcement was varied from under-reinforced to over-reinforced conditions by changing the bottom bar diameter (D12 to D29). Each beam was reinforced with three bottom bars, two Ø8 mm top bars, and Ø6 mm stirrups as transverse reinforcement. Details are shown in Figure 1 and summarized in Table 1.

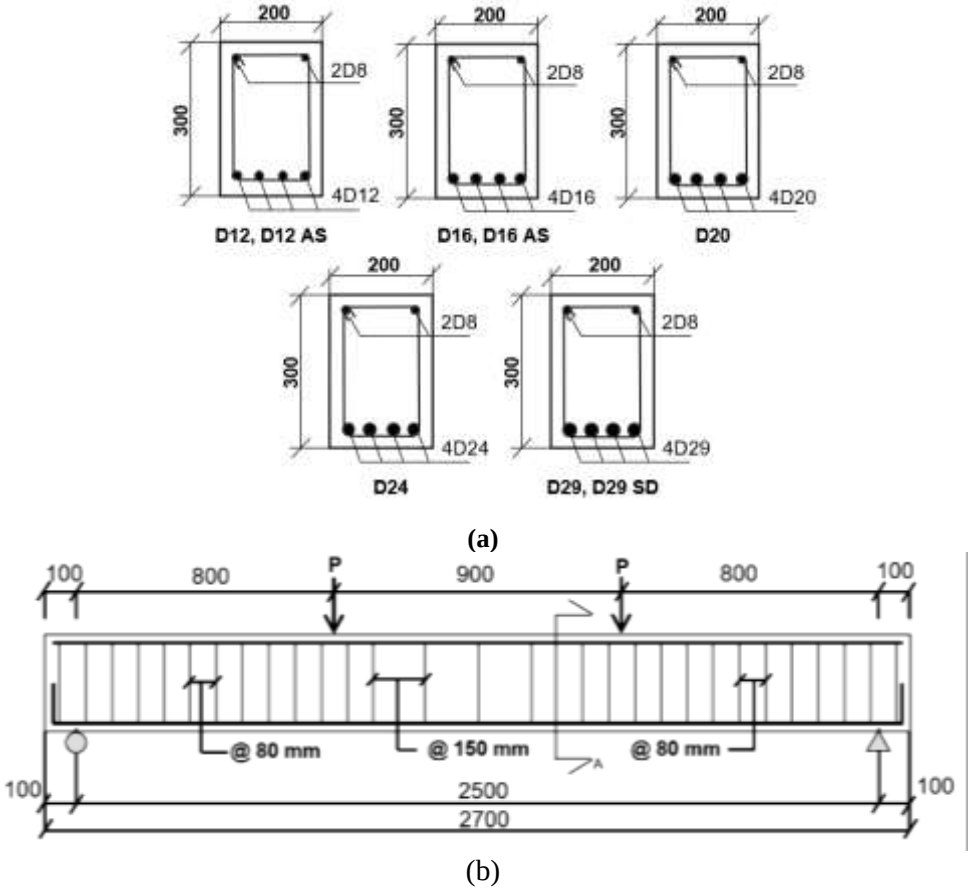

Figure 1. Dimensions and steel reinforcement details of beams: (a) Longitudinal rebar configuration; and (b) Stirrup configuration

Table 1. Reinforcement Ratios

Long. Rebar	As	ρ_{min}	ρ_{max}	ρ_{used}	note
4D12	339.290	0.0083	0.025	0.0057	under reinforced
4D16	603.186	0.0097	0.025	0.01005	balanced
4D20	942.478	0.0110	0.025	0.01571	balanced
4D24	1357.16	0.0110	0.025	0.02262	balanced
4D29	1981.56	0.0110	0.025	0.03303	over reinforced

The geopolymer concrete material model used a compressive strength of 33.16 MPa, tensile strength of 3.5 MPa, and fracture energy of 120 N/m, consistent with previous studies [5], [15]. Steel reinforcement properties are listed in Table 2, and concrete material properties are summarized in Table 3.

Table 2. Steel Reinforcement Properties

Diameter (mm)	Fy (MPa)	fu (MPa)	Es (GPa)	εy	εu
Ø6	238.5	322.5	205.5	0.0012	0.0232
D8	360.4	524.2	205.5	0.0018	0.0351
D12	356.5	527.4	205.5	0.0017	0.0347
D16	415.6	552.6	205.5	0.0020	0.0404
D20	474.7	577.8	205.5	0.0023	0.0462
D24	474.7	577.8	205.5	0.0023	0.0462
D29	474.7	577.8	205.5	0.0023	0.0462

Table 3. Geopolymer Concrete Material Properties

Property	Symbol	Value	Unit
Compressive Strength	f'c	33.16	MPa
Elastic Modulus	Ec	25,000	MPa
Poisson's Ratio	ν	0.2	—
Tensile Strength	ft	3.5	MPa
Fracture Energy	Gf	120	N/m

Ductility was quantified using a displacement-based ratio ($\mu = \delta_U/\delta_y$), where δ_y is the displacement at 70% of peak load and δ_U at 85% of peak load. Total energy absorption (EA) was calculated from the area under the load–deflection curve. The toughness index i_{10} was evaluated following Sharma and Khaloo [16], comparing total work up to $5.5\delta_y$ to elastic work at yield.

$$\mu = \frac{\delta_U}{\delta_y} \tag{1}$$

$$EA = \sum_{i=1}^{n-1} \frac{|P_i| + |P_{i+1}|}{2} \cdot |\delta_i - \delta_{i+1}| \tag{2}$$

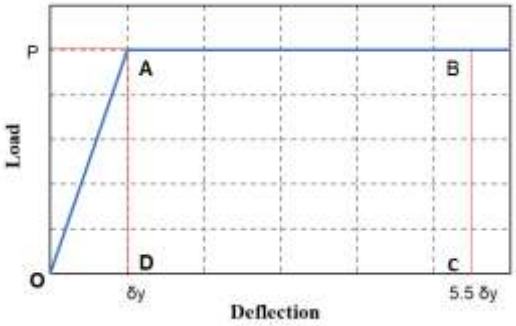

Figure 2. Load-deflection curve for perfectly elasto-plastic material

$$i_{10} = {}^{A_{OABCD}}/_{A_{OAD}} \tag{3}$$

2.2. Preprocessing, Processing, And Post-Processing Finite Element Modeling

Numerical simulation was conducted in three main stages. In preprocessing, geometric modeling and meshing were performed using SALOME. The concrete body was discretized using three-dimensional hexahedral solid elements with a mesh size of 25 mm after sensitivity checks. Reinforcement bars were modeled as wire elements embedded within the solid mesh, with stirrup spacing varied to study shear effects (see Figure 3 for configurations).

(a) Solid Material's Mesh

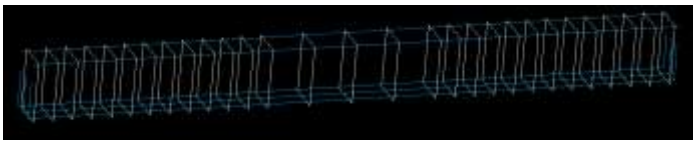

(b) Reinforcement Wire Element

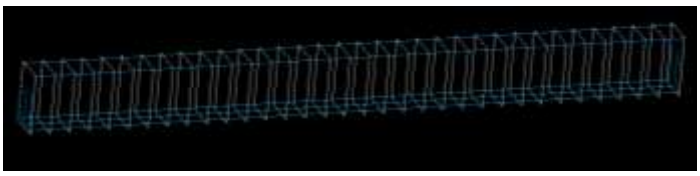

(c) Shear Dominant (SD) Reinforcement Wire Element

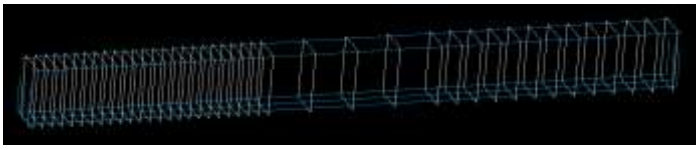

(d) Asymmetric (AS) Reinforcement Wire Element

Figure 3. Geometry Model

During processing, the analysis was executed using 3D Nonlinear Finite Element Analysis (3DNLFEA) software under displacement-controlled monotonic loading, capturing nonlinearities in both concrete and steel until peak load and post-peak softening.

In post-processing, results were visualized using ParaView to examine stress contours and crack propagation. Load–deflection curves were plotted using Gnuplot for comparison of stiffness, peak load, and ductility. This integrated workflow ensured a consistent numerical process tailored to the mechanical characteristics of high-calcium fly ash geopolymer concrete [14], [16].

3. Results and Discussion

Figure 4 shows the load-deflection responses of all eight beams, illustrating how variations in reinforcement ratio influence stiffness, peak load, and post-peak behavior. The results confirm a fundamental trade-off: increasing the longitudinal reinforcement ratio enhances flexural strength but significantly reduces ductility and energy absorption. This trend is consistent with reinforced concrete behavior but occurs at lower reinforcement ratios for high-calcium fly ash geopolymer concrete compared to ordinary Portland cement concrete [14].

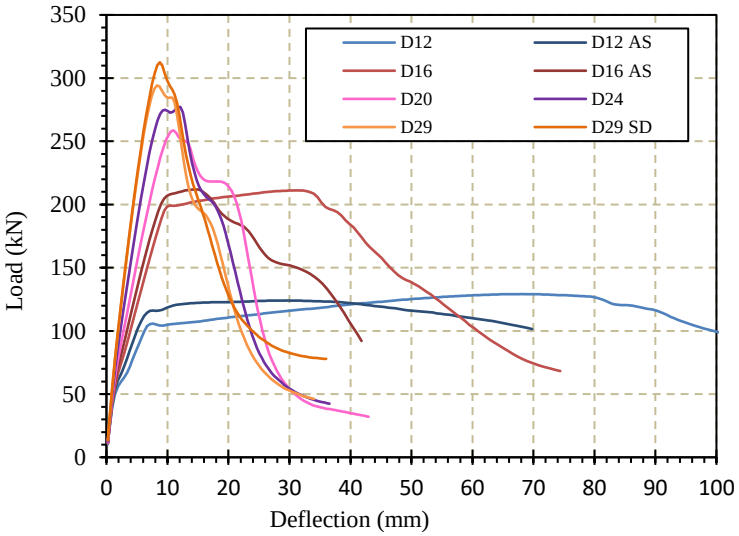

Figure 4. Load–deflection curves for all beam specimens

During initial loading, all beams responded elastically until the tensile capacity of the geopolymer matrix was reached. After cracking, beams with lower reinforcement ratios (D12 and D16) exhibited gradual stiffness reduction and sustained larger deflections before peak load, reflecting ductile, tension-controlled behavior. In contrast, beams with higher reinforcement ratios (D20, D24, and D29) showed abrupt stiffness loss and brittle, compression-controlled failure. The D29 SD specimen, with tighter stirrup spacing, achieved slightly higher strength but maintained similarly brittle post-peak response, demonstrating that increased shear confinement cannot restore flexural ductility once the section is heavily reinforced.

(a)

(b)

Figure 5. (a) D12 at 20.7 mm; (b) D12 at Pmax

(a)

(b)

Figure 6. (a) D12 AS at 20.7 mm; (b) D12 AS at Pmax

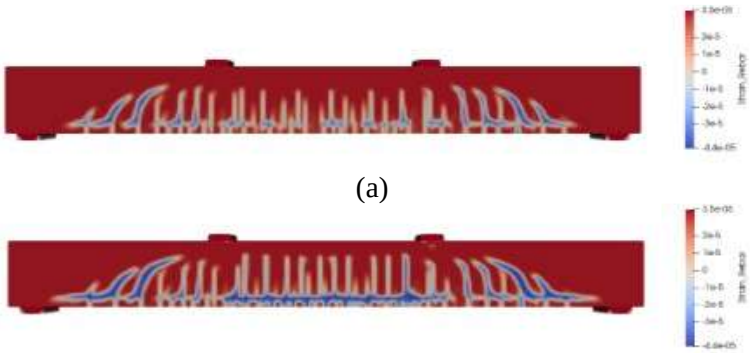

(a)

(b)

Figure 7. (a) D16 at 9.9 mm; (b) D16 at Pmax

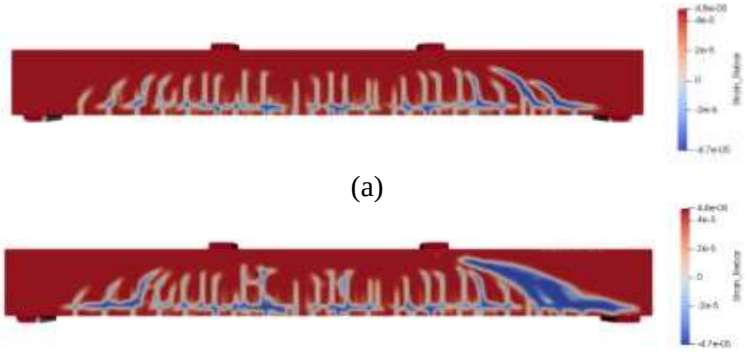

(a)

(b)

Figure 8. (a) D16 AS at 9.9 mm; (b) D16 AS at Pmax

The cracking patterns provide visual evidence of these behavioral differences. The D12 beam (Figure 5) developed widespread flexural cracking along the mid-span at peak load, indicating steel yielding dominated the response. At the same deflection, the asymmetric D12 AS beam (Figure 6) exhibited more concentrated diagonal cracking on the less-confined side, demonstrating how uneven shear reinforcement accelerates localized damage.

Similar trends were observed in beams with balanced reinforcement ratios. The D16 beam (Figure 7) showed dense flexural cracking that transitioned to diagonal patterns, while its asymmetric counterpart (D16 AS, Figure 8) displayed skewed cracking with earlier diagonal shear development. Beams with higher reinforcement ratios exhibited progressively more brittle failure modes.

Figure 9. D20 at Pmax

Figure 10. D24 at Pmax

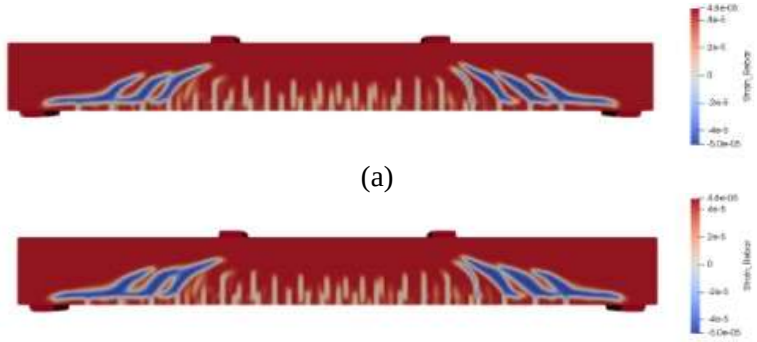

(a)

(b)

Figure 11. (a) D29 at 7.8 mm; (b) D29 at Pmax

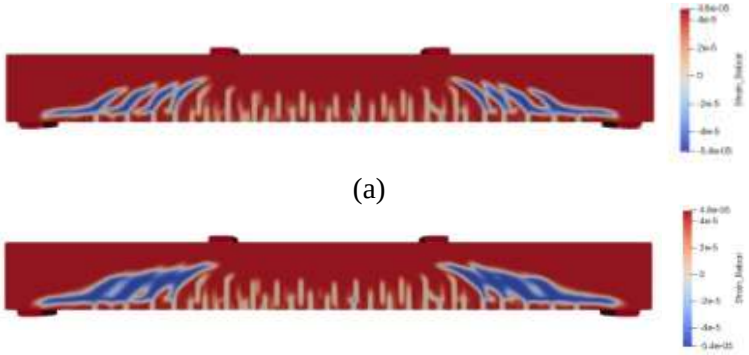

(a)

(b)

Figure 12. (a) D29 SD at 7.8 mm; (b) D29 SD at Pmax

The D20 beam (Figure 9) showed quick transition from fine flexural cracks to deep diagonal cracks, while the D24 beam (Figure 10) displayed fewer but more pronounced diagonal cracks with clear compression crushing.

The D29 beam (Figure 11), intentionally designed as over-reinforced, confirmed this trend with limited flexural cracking followed by rapid diagonal crack formation. The shear-dominated D29 SD configuration (Figure 12) showed vertical cracks quickly developing into concentrated diagonal shear cracks, illustrating how confinement alters failure trajectory without improving ductility.

A key finding is that this ductile-to-brittle transition occurs at significantly lower reinforcement ratios in geopolymer concrete compared to ordinary Portland cement concrete. While design codes such as SNI 2847:2019 [12] permit tension-controlled design up to approximately $\rho = 0.025$ for OPC, the numerical results indicate that brittle failure in this high-calcium fly ash GPC system initiates as early as $\rho = 0.0157$ (D20). This observation aligns with previous studies reporting the limited tensile strain capacity and reduced fracture energy of geopolymer concretes [11], [15], [17].

The ductility ratios provide quantitative evidence of how reinforcement influences the flexural response (Table 4). The under-reinforced D12 and D12 AS specimens developed the highest deformation capacity with ductility values of approximately 13.99 and 12.63. Specimens with balanced reinforcement according to conventional design displayed more varied behavior, with D16 and D16 AS retaining moderate ductility ($\mu = 5.43$ and 4.05). The beams with the highest reinforcement ratios (D24, D29, and D29 SD) demonstrated distinctly brittle response with ductility ratios between 2.41 and 2.70.

Table 4. Ductility Parameters for All Beam Specimens

Specimen	δ_{Pmax} (mm)	P_{max} (kN)	δy (mm)	δu (mm)	μ = δu/δy
D12	68.10	129.14	6.65	93.08	13.99
D12AS	30.20	124.06	5.21	65.74	12.63
D16	31.09	211.17	7.59	41.19	5.43
D16AS	14.66	211.86	5.65	22.87	4.05
D20	11.02	258.60	6.12	16.12	2.63
D24	12.12	277.21	5.18	14.01	2.70
D29	8.28	294.18	4.94	11.93	2.41
D29SD	8.74	312.55	4.71	11.94	2.54

Energy absorption values complement the ductility assessment by quantifying how much external work each beam dissipates during deformation (Table 5). The under-reinforced D12 and D16 beams absorbed the highest amounts of energy (4331.66 N·mm and 848.42 N·mm respectively), reflecting their ability to undergo extensive deformation after cracking. A sharp reduction occurs once reinforcement exceeds the balanced range, with D20, D24, and D29 beams dissipating only 98–130 N·mm despite their higher peak loads.

Table 5. Energy Absorption and i_{10} Index from Load–Deflection Curves.

Specimen	δy (mm)	EA (N.mm)	A_{OAD}	A_{OABCD}	i_{10}
D12	6.65	4331.656	457.29	3770.13	8.24
D12AS	5.21	2160.940	357.35	3190.10	8.93
D16	7.59	848.416	845.78	7671.98	9.07
D16AS	5.65	261.574	587.72	5451.56	9.28
D20	6.12	129.951	588.12	5529.19	7.34
D24	5.18	98.132	588.12	5260.74	7.70
D29	4.94	71.104	796.58	4896.49	6.15
D29SD	4.71	71.264	805.31	4764.90	5.92

To further characterize post-yield deformation capacity, the toughness index i_{10} was evaluated following the method by Sharma and Khaloo [16]. The under-reinforced specimens D12 and D12 AS show i_{10} values of 8.24 and 8.93, reflecting substantial post-yield deformation. As reinforcement increases toward the balanced condition, the D16 beam achieves the highest i_{10} value of 9.07. Once reinforcement increases beyond this level, i_{10} values decline progressively, with D29 and D29 SD falling to 6.15 and 5.92, indicating markedly reduced plastic deformation capacity.

These combined results indicate that high-calcium fly ash geopolymer concrete transitions to brittle failure at reinforcement ratios significantly lower than those permitted for OPC concrete. While SNI 2847:2019 [12] allows tension-controlled design up to approximately $\rho = 0.025$, brittle behavior in this GPC system initiates at $\rho \approx 0.0157$. Therefore, for the material studied ($f'c = 33.16$ MPa), a conservative design limit of $\rho \leq 0.010$ (1.0%) is recommended to ensure ductile, tension-controlled flexural performance.

4. Conclussion

This study numerically investigated the influence of longitudinal reinforcement ratio on the flexural behavior of high-calcium fly ash geopolymer concrete (GPC) beams using three-dimensional nonlinear finite element analysis. The results demonstrate that reinforcement ratio governs the failure

mode of GPC beams, revealing a clear trade-off between flexural strength and ductility. Increasing reinforcement enhances load-carrying capacity but significantly reduces deformation ability and energy absorption. Under-reinforced beams exhibited ductile, tension-controlled failure characterized by steel yielding and distributed cracking, whereas over-reinforced beams failed in a brittle manner due to concrete crushing.

A key finding is that the ductile-to-brittle transition in GPC occurs at substantially lower reinforcement ratios compared to ordinary Portland cement concrete. While conventional design codes such as SNI 2847:2019 [12] permit tension-controlled design up to approximately $\rho = 0.025$ for OPC, this study shows that high-calcium fly ash GPC begins to exhibit brittle behavior at approximately $\rho = 0.0157$. Beams with reinforcement ratios typically classified as balanced in OPC systems displayed compression-controlled failures with limited ductility, indicating that code-based balanced limits are not directly applicable to GPC.

Reinforcement detailing also plays a significant role in structural performance. Asymmetric shear reinforcement layouts resulted in uneven confinement, earlier stiffness degradation, and reduced deformation capacity compared to symmetrically detailed beams. Furthermore, shear confinement alone cannot restore flexural ductility in over-reinforced GPC beams. Although closer stirrup spacing improved diagonal crack resistance and slightly increased load capacity, it did not prevent brittle failure once the longitudinal reinforcement ratio exceeded the ductility threshold.

Based on the consistent trends observed in crack development, load-deflection response, and quantitative ductility metrics, a revised design limit is recommended for high-calcium fly ash GPC. To ensure tension-controlled behavior and adequate ductility, a maximum longitudinal reinforcement ratio of $\rho \leq 0.010$ (1.0%) is proposed for the GPC mix studied. This conservative limit reflects the material's lower tensile strain capacity and earlier transition to brittle failure compared to OPC systems. These findings provide a basis for the development of performance-based design guidelines for geopolymer concrete structures and highlight the need for code provisions that account for the distinct mechanical behavior of GPC.

Acknowledgments

The authors would like to thank the Concrete and Structural Materials Laboratory, Civil Engineering Department, Institut Teknologi Sepuluh Nopember (ITS) Surabaya, for providing the computational facilities and technical support necessary for this research. Special appreciation is extended to Mr. Bambang Piscesa for his guidance and supervision throughout this study. The authors also acknowledge Mr. Indra Komara from ITATS Surabaya for his valuable assistance in manuscript preparation. The constructive feedback from the anonymous reviewers is gratefully acknowledged.

Reference

[1] J. Davidovits, *Geopolymer Chemistry and Applications*. Geopolymer Institute, 2008.

[2] D. Hardjito and B. V. Rangan, "Development and Properties of Low-Calcium Fly Ash Based Geopolymer Concrete," 2005.

[3] P. Duxson, A. Fernández-Jiménez, J. L. Provis, and G. C. Lukey, "Geopolymer technology: The current state of the art," *J Mater Sci*, vol. 42, no. 9, pp. 2917–2933, 2007.

[4] J. Temuujin, A. van Riessen, and R. Williams, "Influence of calcium content on the mechanical properties of fly ash based geopolymer materials," *J Hazard Mater*, vol. 167, pp. 82–88, 2013.

[5] P. Nath and P. K. Sarker, "Use of OPC-based admixtures for high strength geopolymer concrete," *Procedia Eng*, vol. 125, pp. 657–663, 2015.

[6] N. A. Lloyd and B. V. Rangan, "Geopolymer concrete with fly ash," *Proceedings of the World Congress Geopolymer 2005*, 2010, pp. 163–177.

[7] P. Sarker, "Bond strength of reinforcing steel embedded in fly ash-based geopolymer concrete," *Mater Struct*, vol. 44, pp. 1021–1030, 2011.

[8] P. K. Sarker, S. Kelly, and Z. Yao, "Effect of fire exposure on the properties of geopolymer concrete," *Mater Des*, vol. 63, pp. 584–594, 2013.

[9] K. T. Nguyen, A. Castel, and S. Foster, "Reinforced geopolymer concrete beams: Long-term

behavior and flexural performance," *Eng Struct*, vol. 106, pp. 62–75, 2016.
[10] B. Nematollahi, J. Sanjayan, and F. Shaikh, "Tensile properties of strain-hardening fiber-reinforced geopolymer composites," *Constr Build Mater*, vol. 95, pp. 630–641, 2015.
[11] P. Sarker, "Bond strength of reinforcing steel embedded in fly ash-based geopolymer concrete," *Mater Struct*, vol. 44, pp. 1021–1030, 2011.
[12] Badan Standardisasi Nasional, *SNI 2847:2019 Persyaratan Beton Struktural untuk Bangunan Gedung*, Jakarta, 2019.
[13] American Concrete Institute, *ACI 318-14 Building Code Requirements for Structural Concrete and Commentary*, Michigan, USA, 2014.
[14] A. Wibowo and B. Piscesa, "Numerical modelling of flexural behavior of reinforced geopolymer concrete beams using 3D finite element analysis," *Journal of Civil Engineering*, vol. 38, no. 2, pp. 50–67, 2025.
[15] A. Hillerborg, "Analysis of fracture of concrete beams and slabs," *Cem Concr Res*, vol. 6, no. 6, pp. 773–782, 1976.
[16] U. K. Sharma and A. R. Khaloo, "Evaluation of ductility in reinforced concrete members," *ACI Struct J*, vol. 89, no. 4, pp. 397–406, 1992.
[17] V. Pham, "Flexural ductility of geopolymer reinforced concrete beams," *Structures*, vol. 34, pp. 2563–2574, 2021.